

THREE-DIMENSIONAL SEISMIC IMAGING OF EASTERN RUSSIA

Haijiang Zhang^{1,2}, Kevin G. Mackey³, Kazuya Fujita³, Clifford H. Thurber¹, Lee K. Steck⁴,
Charlotte A. Rowe⁴, Steven Roecker⁵, and M. Nafi Toksoz²

University of Wisconsin-Madison¹, Massachusetts Institute of Technology², Michigan State University³,
Los Alamos National Laboratory⁴, and Rensselaer Polytechnic Institute⁵

Sponsored by National Nuclear Security Administration

Contract No. DE-FC52-06NA27325¹⁻³ and DE-AC52-06NA25396⁴
Proposal No. BAA06-77

ABSTRACT

Eastern Russia is composed of a series of terranes which have been accreted to the Precambrian North Asian (Siberian) craton. In the southern part (Baikal and Amur regions), the terranes form a suture zone between the North Asian and North China cratons, which is being exploited by the present-day boundary between the Eurasian plate and the Amur block. The northern part (Magadan and eastern Yakutsk regions) is composed of a series of terranes that accreted to the North Asian craton, primarily in the Mesozoic. This accretionary region is currently the location of the plate boundary between the North American and Eurasian plates. The complexities of accretion and subsequent intracontinental deformation likely result in a highly heterogeneous crust, a broad zone of deformation, and the formation of small blocks or microplates within the ancient suture and present-day plate boundary zones. We assembled catalog picks from ~13,000 events and ~100 stations for the Baikal and Amur regions in the period of 1970 to 2005. For the Magadan and Yakutsk regions, we assembled catalog picks from 3,170 events recorded at 56 stations. Each event has at least 8 P and S observations in order to reliably determine its location. Using the double-difference tomography method (Zhang and Thurber, 2003, 2006), our study for the first time provides a detailed seismic velocity model of the crust and upper mantle for this complicated area. The velocity models in Baikal and Amur regions, as reported in Zhang et al., (2007), show greater heterogeneities at shallow depths, as expected from the variable and complicated nature of the crust. Some Cenozoic and Quaternary rift-related basins around Lake Baikal such as the Upper Angara (northeast) and Tunka (southwest) basins correlate very well to strong low-velocity anomalies. The preliminary velocity models in the Magadan and Yakutsk regions also show strong heterogeneities in the crust. We also determined the Pn velocity model for eastern Russia using Hearn's Pn tomography code.

In our data set, many arrivals at larger distances are identified in the catalog as Pg or Sg phases, which are often observable because of their relatively large amplitudes. Without knowing detailed Moho depth variations, it is not possible to combine both Pn and Sn and Pg and Sg times together. Here we propose a simple way to use Pg and Sg times. From previous studies, the crustal thickness in this region is believed to be generally greater than 35 km. Therefore, in the starting velocity model we introduce an artificial lower-velocity region below 35 km. In this way, the ray paths will stay in the region above 35 km so that they correspond to Pg and Sg phases. During the inversion, we monitored each ray path to make sure it did not penetrate below 35 km. In this way, we can run separate inversions using first and secondary arrivals.

In our tomography algorithm, we use either the spherical-Earth finite-difference (SEFD) travel time method or the spherical pseudo-bending approach of Koketsu and Sekine (1998) to calculate travel times and trace rays. To improve the accuracy and efficiency of the ray tracing, we also adopt a hybrid approach. First, we utilize the FD method with a coarser grid interval to calculate an approximate ray path. Next we start bending this approximate ray path with the spherical pseudo-bending approach until it converges to the desired accuracy. In addition to event-pair differential times used in the double-difference tomography method, we also add station-pair differential times to the tomography algorithm to improve the resolution near the station region.

Report Documentation Page

Form Approved
OMB No. 0704-0188

Public reporting burden for the collection of information is estimated to average 1 hour per response, including the time for reviewing instructions, searching existing data sources, gathering and maintaining the data needed, and completing and reviewing the collection of information. Send comments regarding this burden estimate or any other aspect of this collection of information, including suggestions for reducing this burden, to Washington Headquarters Services, Directorate for Information Operations and Reports, 1215 Jefferson Davis Highway, Suite 1204, Arlington VA 22202-4302. Respondents should be aware that notwithstanding any other provision of law, no person shall be subject to a penalty for failing to comply with a collection of information if it does not display a currently valid OMB control number.

1. REPORT DATE SEP 2008		2. REPORT TYPE		3. DATES COVERED 00-00-2008 to 00-00-2008	
4. TITLE AND SUBTITLE Three-Dimensional Seismic Imaging of Eastern Russia				5a. CONTRACT NUMBER	
				5b. GRANT NUMBER	
				5c. PROGRAM ELEMENT NUMBER	
6. AUTHOR(S)				5d. PROJECT NUMBER	
				5e. TASK NUMBER	
				5f. WORK UNIT NUMBER	
7. PERFORMING ORGANIZATION NAME(S) AND ADDRESS(ES) University of Wisconsin -Madison, Madison, WI, 53704				8. PERFORMING ORGANIZATION REPORT NUMBER	
9. SPONSORING/MONITORING AGENCY NAME(S) AND ADDRESS(ES)				10. SPONSOR/MONITOR'S ACRONYM(S)	
				11. SPONSOR/MONITOR'S REPORT NUMBER(S)	
12. DISTRIBUTION/AVAILABILITY STATEMENT Approved for public release; distribution unlimited					
13. SUPPLEMENTARY NOTES Proceedings of the 30th Monitoring Research Review: Ground-Based Nuclear Explosion Monitoring Technologies, 23-25 Sep 2008, Portsmouth, VA sponsored by the National Nuclear Security Administration (NNSA) and the Air Force Research Laboratory (AFRL)					
14. ABSTRACT see report					
15. SUBJECT TERMS					
16. SECURITY CLASSIFICATION OF:			17. LIMITATION OF ABSTRACT	18. NUMBER OF PAGES	19a. NAME OF RESPONSIBLE PERSON
a. REPORT	b. ABSTRACT	c. THIS PAGE			
unclassified	unclassified	unclassified	Same as Report (SAR)	10	

OBJECTIVES

The objectives of this project are to investigate and develop new and improved methodologies for regional-scale three-dimensional (3D) seismic tomography using a combination of event- and station-pair arrival time differences, and to apply the new methods to the Michigan State University (MSU) and Los Alamos National Laboratory (LANL) Siberia database. The tomographic work proposed here will provide a more reliable velocity model for both the crust and upper mantle of the accretionary regions to the south and east of the Siberian craton. There are four main tasks in this project: (1) an extension of our development of double-difference (DD) seismic tomography to the use of station-pair residual differences, including the incorporation of a new method for resolution matrix calculation; (2) testing, refinement, and adaptation of a method for SEFD travel time calculations for use in DD tomography; (3) an extension of our Cartesian adaptive-grid DD tomography algorithm to spherical coordinates; and (4) collaborative work among the UW-Madison, LANL, and MSU groups to apply these analysis tools to the Siberia data set. In the 2nd year of this project, our focus is to assemble a data set for the Magadan and eastern Yakutsk regions, incorporate station-pair residual differences into the DD seismic tomography algorithm, and determine 3D P- and S-wave velocity models for the Magadan and eastern Yakutsk Baikal regions.

RESEARCH ACCOMPLISHED

Determining the Velocity Model for the Magadan and Eastern Yakutsk regions

Northeast Russia is composed of a large number of terranes of various affinities that have accreted onto the deformed margin of the North Asian (Siberian) Craton (Figure 1; e.g., Fujita et al., 1997; Nokleberg et al., 2000). The diverse nature of the terranes and the evolution of the region over time have resulted in a very heterogeneous crust with potentially abrupt changes in its characteristics. The North Asian Craton is composed of an Archean and Early Proterozoic metamorphic basement overlain by flat-lying Precambrian to Cenozoic sediments. Adjacent to the craton is a deformed margin consisting primarily of Paleozoic to mid-Mesozoic passive margin sediments, thickening to the east, which have been back-thrust onto the margin of the craton. Further east are a series of complexes and terranes that have accreted onto the margin of the North Asian Craton since the mid-Mesozoic. The Verkhoyansk Complex is composed of distal passive margin sequences and oceanic fragments that have been disrupted, deformed, and juxtaposed. The Kolyma-Omolon superterrane consists of a number of cratonal (Omolon, Prikolyma), continental margin (Omulevka), island arc (Alazeya, Khetachan), and oceanic terranes of diverse ages that amalgamated in the Early Mesozoic. In the far northeast of the study area is the Paleozoic to Early Mesozoic Chukotka passive margin terrane that may have formed along the margin of the North America Craton, rifted, and deformed when it collided with the Asian continent along the South Anyui Suture in the Cretaceous. In the south-central part of the study area is the Precambrian Okhotsk cratonal terrane. Southeast of the Okhotsk terrane and the Verkhoyansk complex is the Jurassic to Cretaceous Uda-Murgal island arc that accreted onto the Asian continent in the mid-to-late Cretaceous. Superimposed on all of the previously described units is the Okhotsk-Chukotka volcanic belt (Figure 1), a continental margin volcanic arc. Further complicating crustal and lithospheric structure in the region are a series of post accretionary extensional and compressional events that have affected the region since the Late Cretaceous, and the superposition and migration of the plate boundary between North America and Eurasia across northeast Russia in the Cenozoic (Fujita et al., 1990). In particular, Late Cenozoic rifting appears to have had significant impact on crustal and upper mantle structure.

We assembled catalog picks from 3,170 events recorded at 56 stations in the region bounded by latitudes 58°–75° and longitudes 115°–165° (Figure 2). Each event has at least 8 P and S observations in order to reliably determine its location. In total, we collected ~19,000 Pn+Pg arrivals and 24,000 Sn+Sg arrivals. Figure 2 also shows P and S ray path distributions. From travel time curves shown in Figure 3, we note there are some outliers in the catalog picks. We cleaned up the P and S times by removing outliers falling outside the major trend of the travel time curves. As a result, we obtained ~3,500 P and ~1,930 S first arrivals corresponding to 628 events. In comparison, there are ~12,690 Pg and ~18,600 Sg times from ~2,640 events because it is easier to pick Pg and Sg phases due to their relatively large amplitudes in the seismograms.

For eastern Russia, the crustal thickness is generally greater than 35 km. In order to use Pg and Sg times that are secondary arrivals, we intentionally add a lower velocity layer below 35 km so that the rays do not tend to penetrate deeper than 35 km. During the inversion, we monitored the maximum penetration depth for each ray path and removed it from the inversion if it penetrated deeper than 35 km. We constructed ~76,000 P and ~123,000 S event-pair differential times directly from catalog picks. For the starting model, we used a crustal model consisting

of 5 km of 5.3–5.8 km/s material overlying 15 km of 6.0 km/s material (“granitic”), and a 20-km thick lower crust of 6.8 km/s (“basaltic”). This yields a 40-km-thick crust which is underlain by 8.0 km/s upper mantle. The grid intervals in the horizontal directions range from 0.5° in the inner part to 2° around the edge of the model. In depth, the grid interval is 5 km. The initial root-mean-square (RMS) arrival time residual is 2.643 s. After 8 iterations of simultaneous inversion of the velocity model and locations, the final RMS arrival time residual is 0.826 s. Figure 4 shows the Vp and Vs models at selected depths.

Pn velocity Tomography for Eastern Russia

We collected 9,630 Pn travel times for 151 stations and 9,630 events from the MSU database (Figure 5). Each event has at least 3 Pn recordings. We followed Hearn’s approach to invert Pn travel time residuals for lateral velocity variation within the mantle lid, event delays, and station delays (Hearn and Ni, 1994). The surface of the uppermost mantle is parameterized into a set of 0.5° by 0.5° cells. The initial RMS Pn travel time residual with respect to the average Pn velocity model of 8 km/s is 1.66 s and the final RMS Pn travel time residual is 1.12 s. Figure 6 shows Pn velocity variations of eastern Russia. Overall, the Siberian platform has higher velocities than the accretionary region.

Differential Time Seismic Tomography Algorithm

Zhang and Thurber (2003) generalized the DD location method of Waldhauser (2001) to determine 3D velocity structure and event locations jointly. The equations for the DD tomography algorithm are

$$r_k^i - r_k^j = \sum_{m=1}^3 \frac{\partial T_k^i}{\partial x_m^i} \Delta x_m^i + \Delta \tau^i + \int_i^k \delta u \, ds - \sum_{m=1}^3 \frac{\partial T_k^j}{\partial x_m^j} \Delta x_m^j - \Delta \tau^j - \int_j^k \delta u \, ds \quad (1)$$

where r_k^i and r_k^j are residuals from events i and j at station k , T 's are travel times, x and Δx are hypocenter coordinates and their perturbations, τ 's are origin times, δu is perturbation to slowness, and ds is an element of path length. Three types of data, absolute arrival times, catalog differential arrival times, and waveform cross-correlation (WCC) data, are used in the inversion. To combine these three types of data into one system, we apply a hierarchical weighting scheme during the inversion, similar to hypoDD (Waldhauser, 2001).

We can also consider a variant of Equation 1 in which we have two different, nearby stations recording a single event:

$$r_j^i - r_k^i = \sum_{m=1}^3 \frac{\partial T_j^i}{\partial x_m^i} \Delta x_m^i + \int_i^j \delta u \, ds - \sum_{m=1}^3 \frac{\partial T_k^i}{\partial x_m^i} \Delta x_m^i - \int_i^k \delta u \, ds \quad (2)$$

where now r_j^i and r_k^i are residuals from event i at stations j and k , and the origin time terms drop out since there is only one event involved. If the stations are sufficiently close, the location derivative terms in Equation 2 cancel, and what remains are slowness perturbation terms along slightly different paths. Phillips et al. (2005) explored the utility of this formulation for the determination of a 2D tomographic model. Their motivation was that, for advantageous geometries, the time difference for arrivals from one event to two stations can be insensitive to location accuracy. For example, for an event in line with (but not between) two stations, much of the ray paths are essentially in common, and the time difference is related to the properties sampled by the additional ray-path length to the more distant station as well as the medium directly under the closer station. This time difference will not change much if the source moves 10 km or even more. There is only a "dipole"-shaped area in between and perpendicular to the line between the two stations where the time differences are not stable and are very sensitive to location. Thus, the time differences provide strong constraints even if the ground truth (GT) levels of the events are poor.

The success of this simplistic approach leads us to propose the formal use of Equation 2 in a 3D tomographic inversion. There is a direct parallel between Equation 1 (DD tomography), in which event-pair time differences provide information about 3D structure in the vicinity of the sources, and Equation 2, in which station-pair time differences provide information about 3D structure in the vicinity of the stations. In the former case, we know that very precise differential times can be derived for closely spaced events, leading to very precise relative event locations and sharply defined structure in the source region. Similarly, we can expect that for closely spaced stations, relative times can be determined more precisely than individual absolute times. Tomography using station-pair residual differences is somewhat akin to teleseismic tomography, but with the sources contained within the model region.

For simplicity, we construct a 2D synthetic model (Figure 7) to show the properties of the inversions with different combinations of event- and station-pair differential arrival times, and/or absolute times. There are six clusters of earthquakes (circles) and each cluster has four closely spaced events with inter-event distances of less than 200 m. In the X- and Y-directions, the distances between clusters are 10 and 15 km, respectively. There are 36 stations around these events, with all the events observed at each station. As a result, there are 894 travel times in total for all the event and station pairs. The velocity is assumed to be constant at 5 km/s; thus, the rays between events and stations are all straight lines. The region is divided uniformly into 81 cells (or blocks). The model derivatives relative to slowness are just the path lengths crossing the cells.

Figures 8a and 9a show model resolution for location and slowness model parameters in the case of using event-pair time differences and station-pair time differences, respectively. These are shown for different combinations of weightings with absolute times. Event-pair and station-pair time differences are constructed for all possible event pairs and station pairs, respectively. For the case of using event-pair time differences (our original version of DD tomography) (Figure 8a), the systems with higher weighting on the differential data seem to better resolve event locations by having higher resolution values (~ 0.7 versus ~ 0.3). For slowness model parameters around the edge of the model, however, the systems having higher weighting on the absolute data have higher model resolution. This is mainly because the ray paths from event pairs outside the source region almost overlap so that the corresponding slowness model derivatives cancel out. This indicates that the absolute times are necessary to resolve the velocity model outside the source region. For the case of using the station-pair time differences (Figure 9a), both location and slowness model parameters have higher resolution for the systems having higher weighting on the differential data than those having higher weighting on the absolute data. When compared to the case of using event-pair differential times, using the station-pair time differences better resolves the structure near the station region.

We assume that the errors associated with both absolute and differential data (both event-pair and station-pair) are an uncorrelated Gaussian-distributed random process. The assumed standard deviations for the absolute and differential data are 80 and 20 ms, respectively. This simulates the scenario that the differential data are more accurate than the absolute data. These values would be representative of absolute catalog picks and differential catalog picks; using the even more precise cross-correlation differential times would obviously make the uncertainty contrast greater. Figures 8b and 9b show the model uncertainties for the cases of using event-pair, station-pair, and event- and station-pair time differences, respectively, including different combinations with absolute times. For the case of using event-pair time differences (Figure 8b), the model uncertainties estimated from the system having higher weighting on the absolute data are much larger, especially for event locations. We also notice that the slowness model cells closer to two model region edges ($X=5$ and 50 km) tend to have larger model uncertainties. This phenomenon results from the relatively smaller number of rays crossing through those cells. The characteristics of model uncertainties for the case of having higher weighting on the differential data (diff and diff+0.01*abs) are quite similar, with the system (diff+0.01*abs) having slightly larger uncertainties for some slowness model cells. We also observe that the model uncertainties, including event locations and slowness model parameters, are smaller for the systems having higher weighting on the differential times in the case of using station-pair time differences (Figure 9b). For the simple synthetic dataset analyzed, including a combination of absolute and differential data provides a better balance between good resolution and low uncertainty compared to using just absolute or differential data alone, as one might expect. We also conducted a resolution and uncertainty analysis in the case of using both event- and station-pair time differences. The results are very similar to the case of using station-pair time differences. This is mainly because the sources are so tightly clustered but the clusters are so far apart, whereas stations are more uniformly separated. The current synthetic model is too simple to represent the real case of proposed regional-scale tomography study where the inter-station and inter-event distances are quite variable and

relatively small compared to ray path lengths. However, this simple test does certainly show that including station-pair time differences helps to better resolve the velocity structure near the station region.

We successfully modified the double-difference tomography code to include the station-pair travel time differences. For the test, we applied it to the data set of Baikal and Amur regions. For this test, we constructed station-pair differences from all possible station pairs for each event. We started the inversion from the velocity model and event locations calculated using absolute and event-pair arrival time differences. The initial RMS station-pair travel time residual is 1.536 s and the final RMS residual is 0.653 s after four iterations of simultaneous inversion. Figure 10 shows the comparison of the velocity models using station-pair and event-pair time differences. The main features of the two velocity models are very similar, but the differences are up to 0.2 km/s. The mean horizontal and vertical location differences are around 1.5 km and 1.3 km, respectively. With the effect of origin times reduced, we expect the locations are more accurate using station-pair travel time differences.

CONCLUSIONS AND RECOMMENDATIONS

We successfully modified the double-difference seismic tomography algorithm to include the station-pair travel time differences. The simple synthetic test showed that including station-pair travel time differences helps to better resolve the velocity structure near the station region. The application to the Baikal and Amur regions also showed the effectiveness of including station-pair travel time differences in resolving the structure in the crust.

We assembled a dataset for northeastern Russia comprising Pn+Pg and Sn+Sg picks. At larger epicentral distances, the Pg and Sg are secondary arrivals and could not be directly used in double-difference seismic tomography. To use Pg and Sg arrivals, we simply added an artificial low-velocity layer below the estimated Moho interface so that the rays only travel in the crust. The velocity model shows strong heterogeneity in the crust for northeastern Russia using Pg and Sg times. We plan to use the adaptive inversion mesh based on tetrahedral diagrams according to the data coverage.

REFERENCES

- Fujita, K., F.W. Cambray, and M.A. Velbel (1990). Tectonics of the Laptev Sea and Moma rift systems, northeastern USSR: *Marine Geology* 93: 95-118.
- Fujita, K., D.B. Stone, P.W. Layer, L.M. Parfenov, and B.M. Koz'min (1997). Cooperative program helps decipher tectonics of northeast Russia, *Eos Trans. Am. Geophys. Union* 78:245,252-253.
- Hearn, T. M., and J. Ni (1994). Pn velocities beneath continental collision zones: The Turkish-Iranian plateau, *Geophys. J. Int.* 117: 273- 283.
- Koketsu, K., and S. Sekine (1998). Pseudo-bending method for three-dimensional seismic ray tracing in a spherical earth with discontinuities, *Geophys. J. Int.* 132: 339-346.
- Nokleberg, W. J., L.M. Parfenov, J.W.H. Monger, B.V. Baranov, S.G. Byalobzhesky, T.K. Bundtzen, T.D. Feeney, K. Fujita, S.P. Gordey, A. Grantz, A.I. Khanchuk, B.A. Natal'in, L.M. Natapov, I.O. Norton, W.W. Jr. Patton, G. Plafker, D.W. Scholl, S.D. Sokolov, G.M. Sosunov, D.B. Stone, R.W. Tabor, N.V. Tsukanov, and T.L. Vallier (2000). Summary Circum-North Pacific tectono-stratigraphic terrane map, *US Geological Survey, Open-File Report: 96-727*, scale 1:10,000,000.
- Phillips, W.S., C.A. Rowe, and L.K. Steck (2005). The use of interstation P wave arrival time differences to account for regional path variability, *Geophys. Res. Lett.* 32: L11301, doi:10.1029/2005GL022558.
- Zhang, H., and C. H. Thurber (2003). Double-difference tomography: the method and its application to the Hayward Fault, California, *Bull. Seism. Soc. Am.*, 93: 1875-1889.
- Zhang, H., and C. Thurber (2006). Development and applications of double-difference tomography, *Pure and Applied Geophys.* 163: 373-403, doi:10.1007/s00024-005-0021-y.
- Zhang, H., K. Mackey, K. Fujita, L. Steck, C. Rowe, C. Thurber, and S. Roecker (2007). High-Resolution Three-Dimensional Seismic Imaging of Baikal and Amur Regions of Eastern Russia, in *Proceedings of the 29th Monitoring Research Review: Ground-Based Nuclear Explosion Technologies*, LA-UR-07-5613, Vol. 1, pp. 333-342.

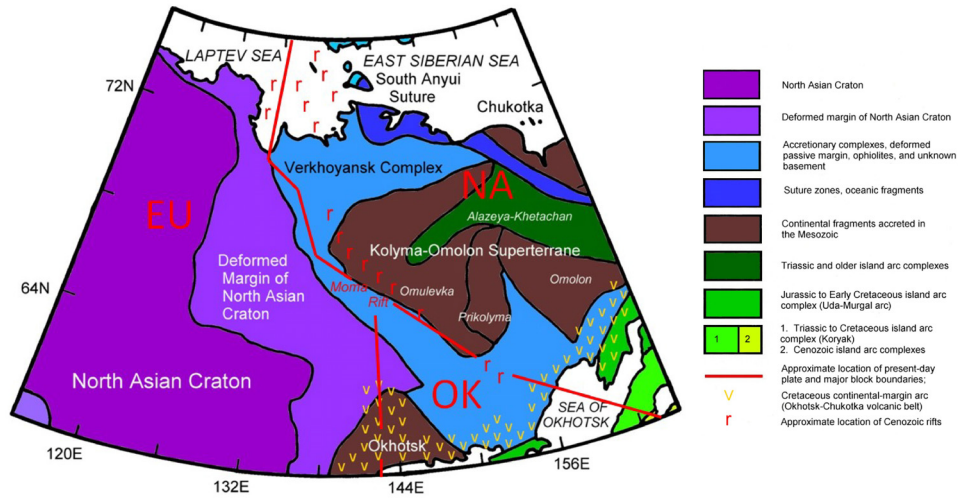


Figure 1. Tectonic map of northeastern Russia.

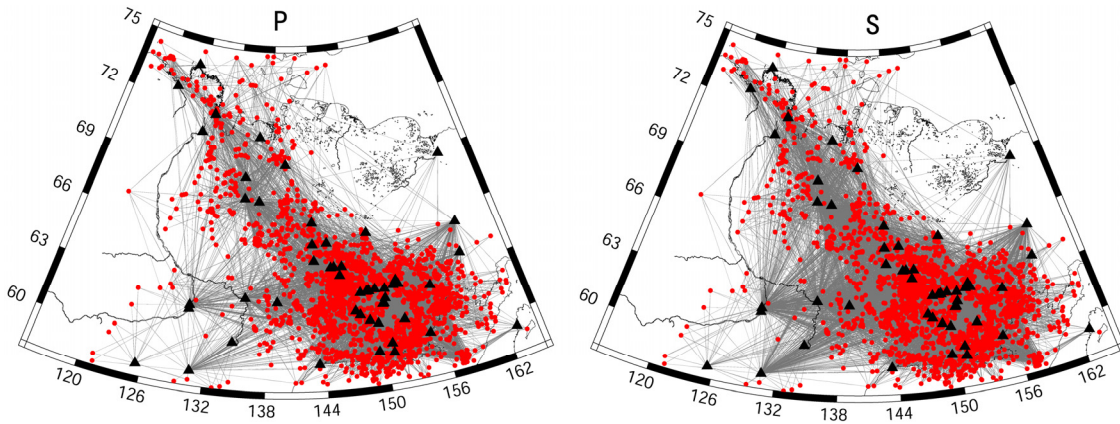


Figure 2. Event-station path coverage for P-waves (left) and S-waves (right). Events are represented in red and stations are in black.

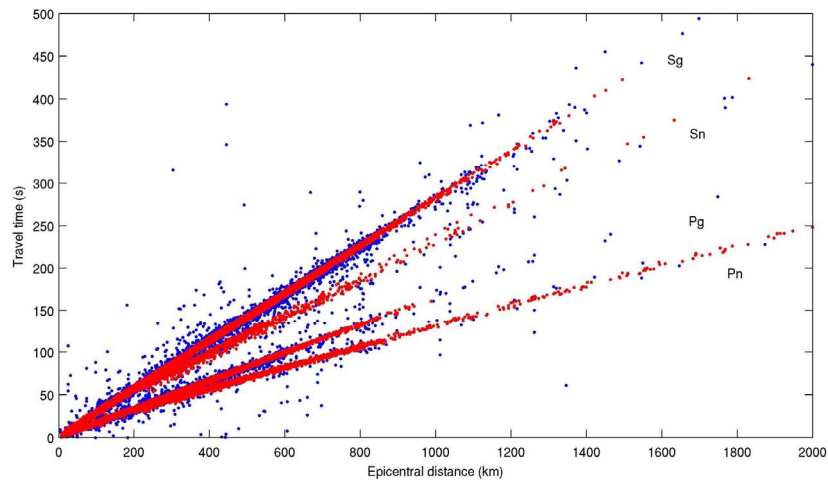


Figure 3. Composite travel time curve. The blue color shows all the picks from the MSU database. The red color indicates the selected picks. The epicentral distance is calculated using original catalog locations.

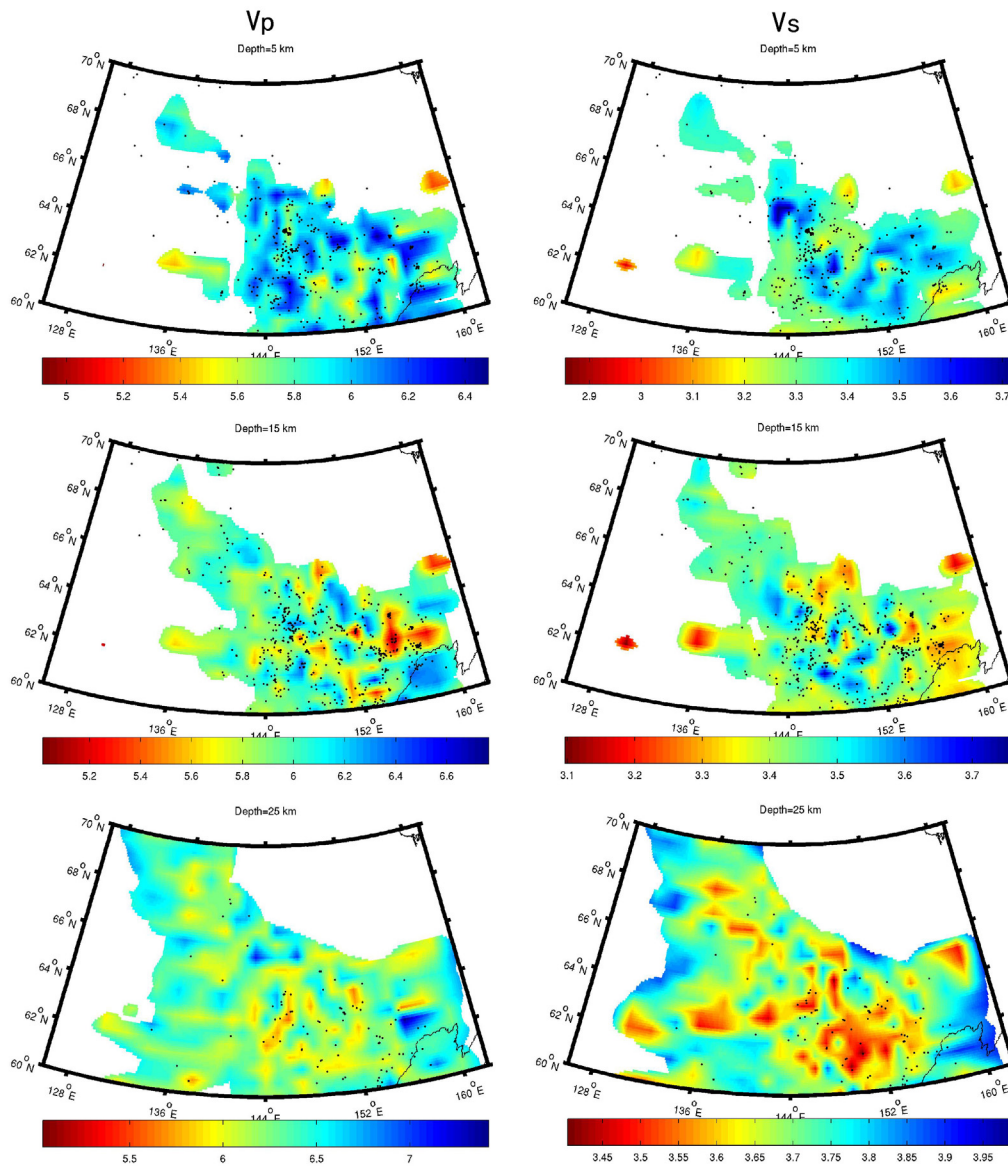


Figure 4. Horizontal slices of Vp and Vs model at depths of 5, 15, and 25 km.

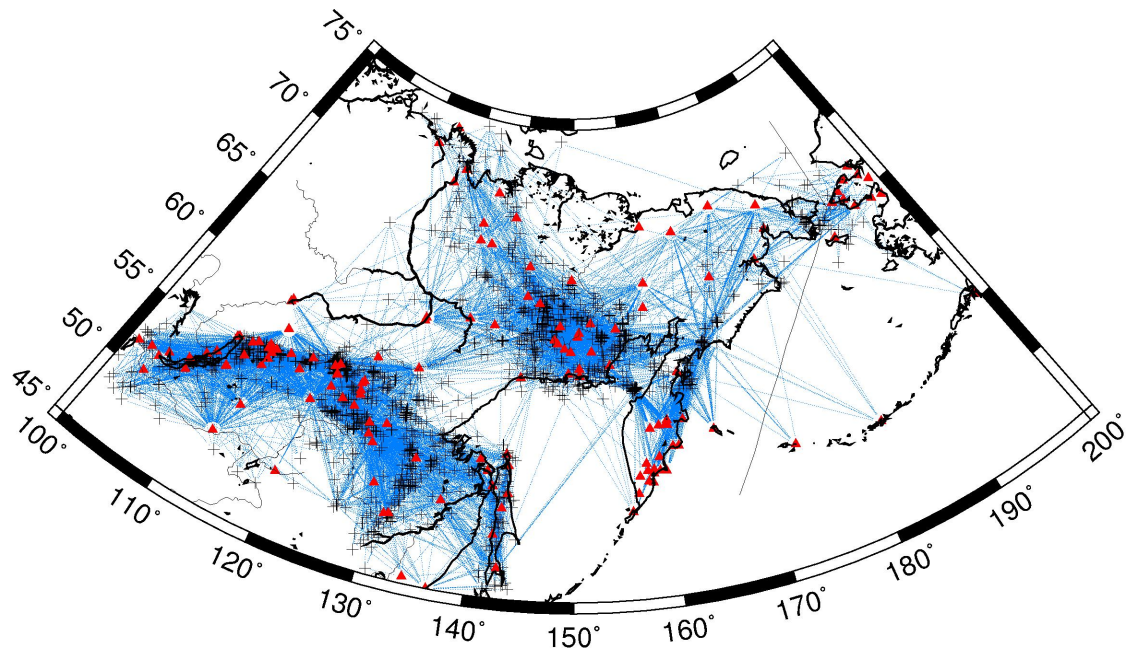


Figure 5. Distribution of 9630 Pn ray paths (blue dashed line) from 1651 events (crosses) and 151 stations (red triangles) for eastern Russia.

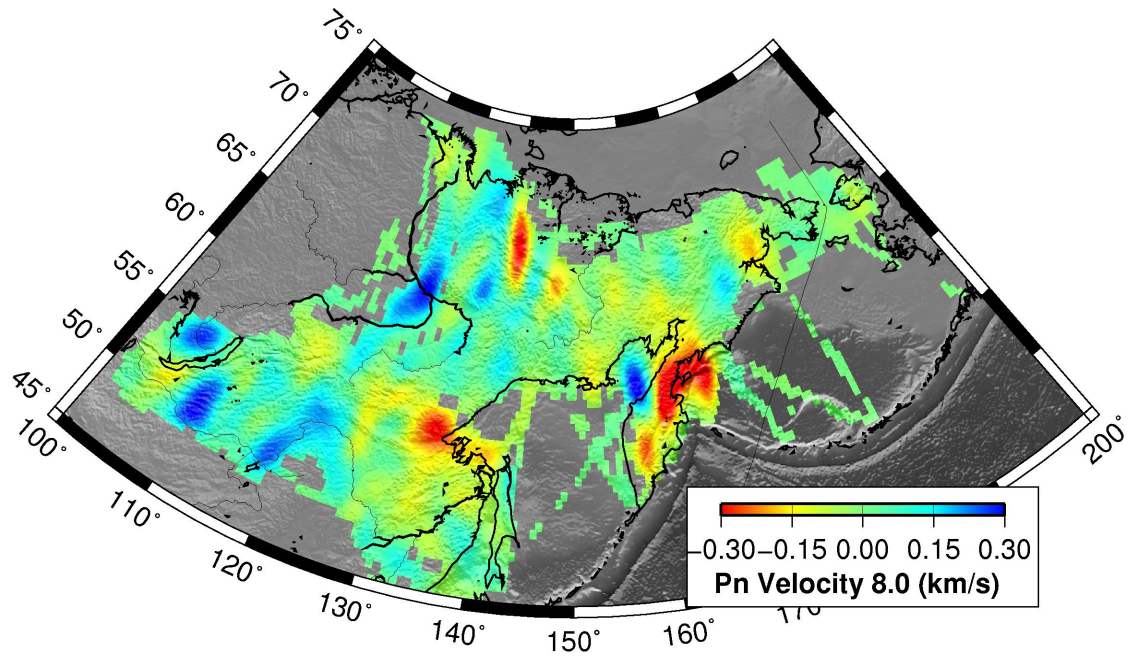


Figure 6. Pn lateral velocity variations. Average Pn velocity is 8.0 km/s. Blue indicates higher velocity and red indicates lower velocity.

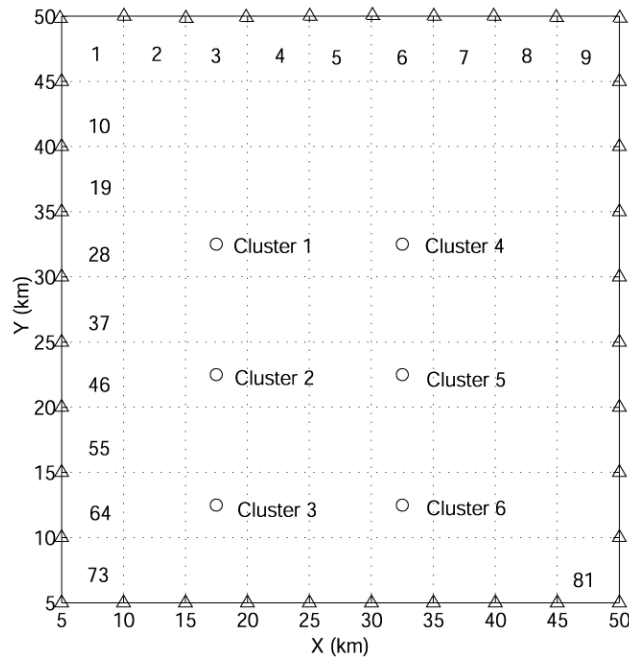


Figure 7. Map of stations (triangles) and earthquake clusters (circles) for the synthetic example. Each cluster has 4 closely spaced events, with interevent distances among them less than 200 m. The velocity model is assumed to be a constant 5 km/s. The model region is divided into 81 cells uniformly, with numbers in the cells indicating the model parameter indices.

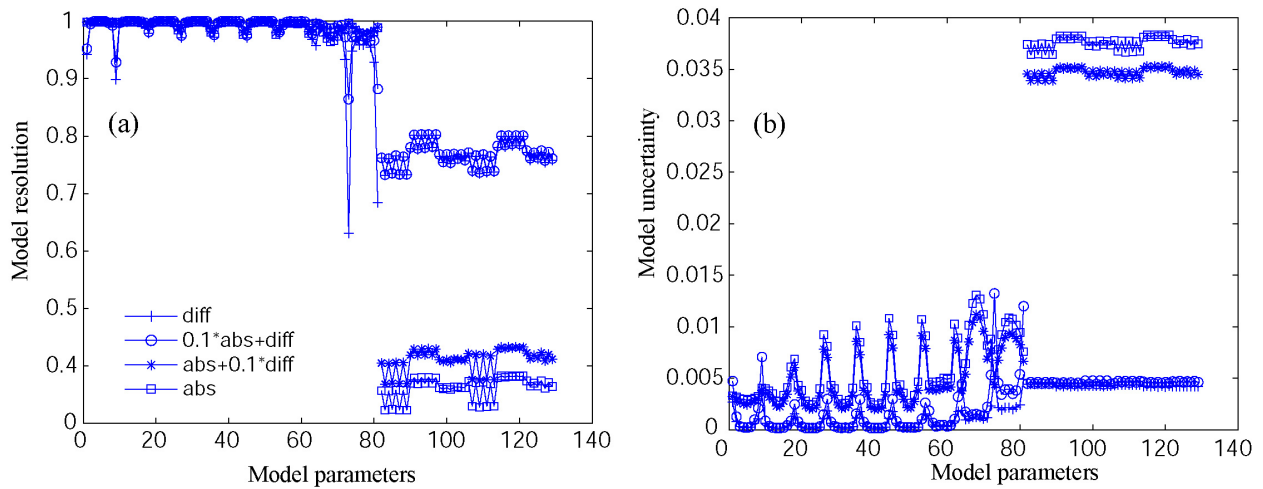


Figure 8. Example of (a) resolution analysis and (b) uncertainty analysis for slowness (model parameters 1 through 81) and location (model parameters 82 through 129) model parameters. Including a combination of absolute and differential data provides a better balance between good resolution and low uncertainty compared to absolute or differential data alone.

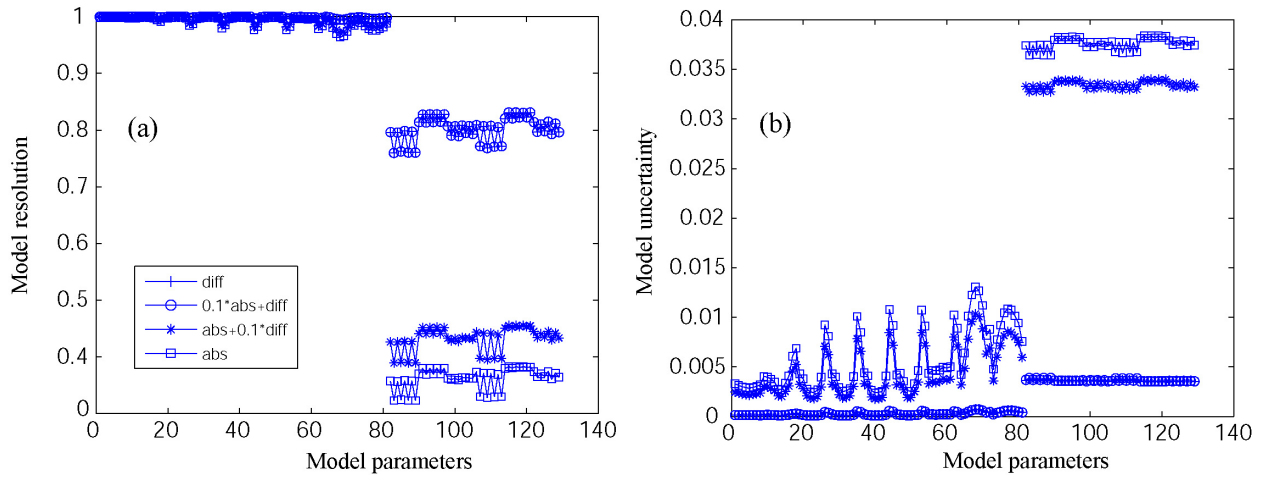


Figure 9. Same as Figure 8 except for using station-pair time differences.

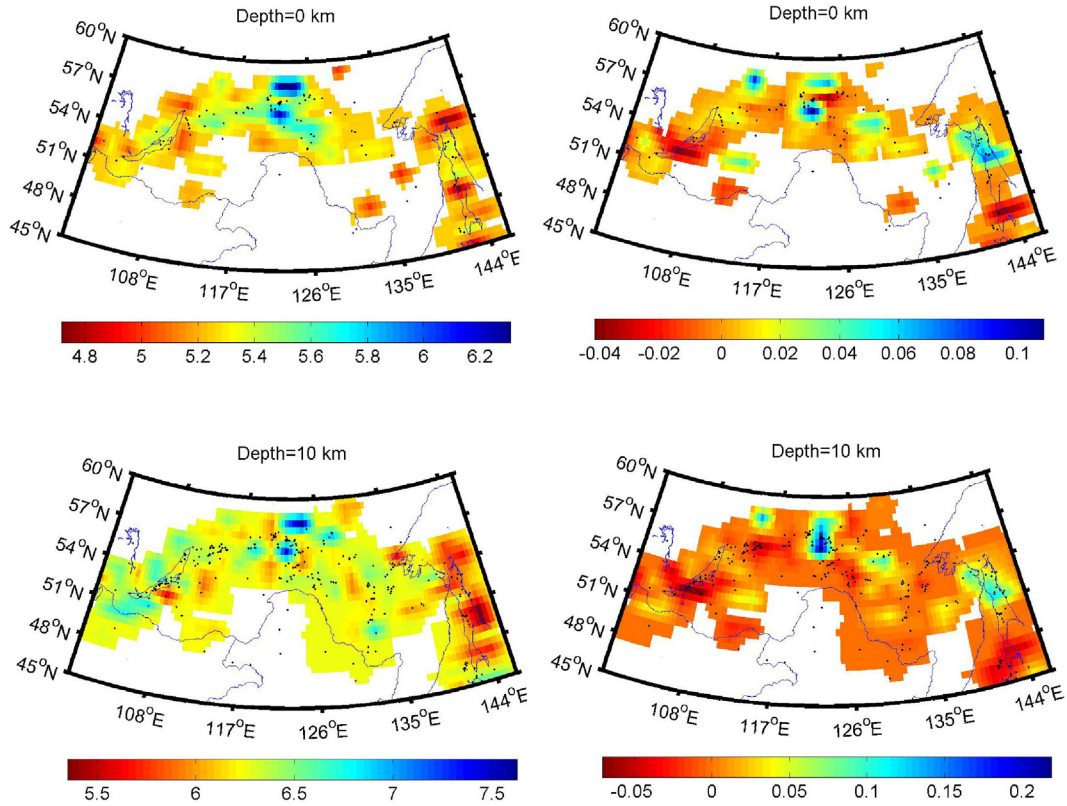


Figure 10. Comparison of the velocity models using event-pair and station-pair time differences. (Left) Horizontal slices of the V_p model from the inversion using station-pair differences. (Right) Differences between velocity models derived from station-pair differences and event-pair differences.